Molecular Therapy
Original Article

Efficient *In Vivo* Liver-Directed Gene Editing Using CRISPR/Cas9

Kshitiz Singh,[1,5] Hanneke Evens,[1,5] Nisha Nair,[1,5] Melvin Y. Rincón,[1,2,3] Shilpita Sarcar,[1] Ermira Samara-Kuko,[1] Marinee K. Chuah,[1,2,4] and Thierry VandenDriessche[1,2,4]

[1]Department of Gene Therapy and Regenerative Medicine, Faculty of Medicine and Pharmacy, Vrije Universiteit Brussel (VUB), 1090 Brussels, Belgium; [2]Center for Molecular and Vascular Biology, Department of Cardiovascular Sciences, University of Leuven, 3000 Leuven, Belgium; [3]Centro de Investigaciones, Fundacion Cardiovascular de Colombia, 681004 Floridablanca, Colombia

***In vivo* tissue-specific genome editing at the desired loci is still a challenge. Here, we report that AAV9-delivery of truncated guide RNAs (gRNAs) and Cas9 under the control of a computationally designed hepatocyte-specific promoter lead to liver-specific and sequence-specific targeting in the mouse *factor IX* (*F9*) gene. The efficiency of *in vivo* targeting was assessed by T7E1 assays, site-specific Sanger sequencing, and deep sequencing of on-target and putative off-target sites. Though AAV9 transduction was apparent in multiple tissues and organs, Cas9 expression was restricted mainly to the liver, with only minimal or no expression in other non-hepatic tissues. Consequently, the insertions and deletion (indel) frequency was robust in the liver (up to 50%) in the desired target loci of the *F9* gene, with no evidence of targeting in other organs or other putative off-target sites. This resulted in a substantial loss of FIX activity and the emergence of a bleeding phenotype, consistent with hemophilia B. The *in vivo* efficacy of the truncated gRNA was as high as that of full-length gRNA. Cas9 expression was transient in neonates, representing an attractive "hit-and-run" paradigm. Our findings have potentially broad implications for somatic gene targeting in the liver using the CRISPR/Cas9 platform.**

INTRODUCTION

CRISPR RNA-guided nucleases (Cas9 nucleases) offer encouraging prospects for efficient genome editing. These molecules have recently been used to target specific genomic loci *in vitro* and *in vivo*, leading to site-specific alterations in the targeted genes.[1–5] CRISPR/Cas9-mediated gene editing triggers a DNA-sequence-specific double-strand[6] DNA break that stimulates gene repair by either non-homologous end joining (NHEJ) or homologous recombination (HR) in the presence of a homologous DNA template. NHEJ can also result in the insertion or deletion of nucleotides at the target locus, resulting in frameshift or nonsense mutations leading to a loss-of-function phenotype. Genome editing using CRISPR/Cas9 has been particularly effective to generate transgenic animals containing specific mutations in the desired target loci through the genetic modification of embryonic stem cells (ESCs)[7,8] or zygotes,[9–12] with broad implications for functional genomics studies. In addition, CRISPR/Cas9 has been used to genetically modify clinically relevant cell types *ex vivo*, including T cells and hematopoietic stem cells,[13,14] induced pluripotent stem cells (iPSCs)[15,16] and other adult stem cells.[17] This impacts the field of regenerative medicine for the treatment of degenerative diseases.[18–20]

In vivo genome editing in post-natal animals, however, has been more challenging. *In vivo* delivery of CRISPR/Cas9 has been achieved using either hydrodynamic delivery or viral transduction with either adenoviral or adeno-associated virus (AAV) vectors.[2,21–26] However, in some cases, the targeting efficiency in somatic cells was relatively modest (<1%)[23] and failed to yield a distinct phenotype. Alternatively, *in vivo* selection was required to enrich for the gene-edited cells,[27] limiting its application to only those genes that conferred a selective growth and survival advantage *in vivo* (e.g., fumarylacetoacetate hydrolase [*Fah*]). In particular, this limited efficiency was compounded by the limited packaging capacity of AAV vectors and the relatively large size of the conventional codon-usage optimized *Streptococcus pyogenes* Cas9 (~4.2 kb), necessitating the use of smaller promoters that were either relatively weak and/or not tissue specific.[23] The use of adenoviral vectors for *in vivo* editing using CRISPR/Cas9 hampers ultimate clinical translation, given its known inflammatory properties following systemic administration that often provoke liver toxicity and rapid immune clearance of gene-modified cells.[28] In addition, most of the adenoviral vector-based genome editing studies used a ubiquitously expressed cytomegalovirus (*CMV*) promoter to drive the Cas9 protein, increasing the likelihood of undesired genome editing in non-target tissues. Finally, all of the previously published *in vivo* editing studies relied on the use of non-truncated guide RNAs (gRNAs), which are known to yield a higher frequency of non-specific

Received 21 December 2015; accepted 21 February 2018;
https://doi.org/10.1016/j.ymthe.2018.02.023.

[4]These authors contributed equally to this work.

[5]These authors contributed equally to this work.

Correspondence: Thierry VandenDriessche, Department of Gene Therapy and Regenerative Medicine, Faculty of Medicine and Pharmacy, Vrije Universiteit Brussel (VUB), Building D, Room D365, Laarbeeklaan 103, 1090 Brussels, Belgium.
E-mail: thierry.vandendriessche@vub.be
Correspondence: Marinee K. Chuah, Department of Gene Therapy and Regenerative Medicine, Faculty of Medicine and Pharmacy, Vrije Universiteit Brussel (VUB), Building D, Room D365, Laarbeeklaan 103, 1090 Brussels, Belgium.
E-mail: marinee.chuah@vub.be

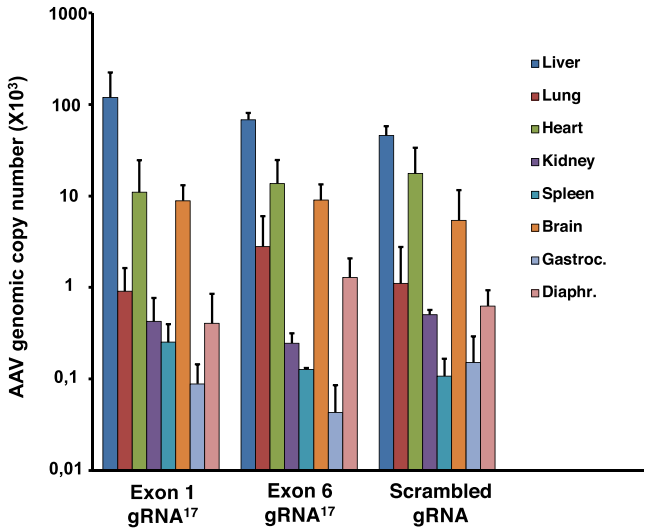

Figure 1. AAV Copy Number in Liver, Lung, Heart, Kidney, Spleen, Brain, Gastrocnemius Muscle, and Diaphragm

The AAV9-HS-CRM8-TTRmin-Cas9 vector (6.25×10^{10} vg/mouse i.v.) was co-injected with either the AAV9-U6-mF9-Exon1-gRNA[17], AAV9-U6-mF9-Exon6-gRNA[17], or control AAV9-U6-scrambled-gRNA vectors (1.25×10^{11} vg/mouse i.v.). Vector copy number (mean ± SD) was determined by qPCR using primers specific for the synthetic liver-specific *HS-CRM8-TTRmin* promoter driving Cas9 expression.

off-target editing,[29,30] as confirmed following somatic *in vivo* editing.[31] These limitations justify the development and validation of robust tissue-specific *in vivo* gene editing platforms that further minimize the risk of off-target gene editing in non-target genes and/or non-target tissues. In this study, we address these limitations and validated an improved CRISPR/Cas9-based AAV platform[32,33] capable of achieving efficient and stable liver-specific genome editing *in vivo* with a potentially reduced risk of off-target effects in non-target genes while also preventing gene targeting in non-target organs.

RESULTS

Selection of gRNA Target Sites and Design of the Liver-Specific AAV9-Cas9 Vector

Truncated and full-length gRNAs were specifically designed to target the murine *factor IX* (*F9*) gene using CRISPR/Cas9, taking into account the following considerations: (1) the target sites were selected at the 5′ end of the *F9* gene, making it more likely to generate a non-functional coagulation factor IX (FIX) protein by introducing frameshift mutations following NHEJ;[18] (2) the target sites overlap with mutations known to cause hemophilia B in patients, based on the human FIX database (http://www.factorix.org/); and (3) the selected gRNAs were subjected to a genome-wide analysis using a computational BLAST tool (Ensembl; NCBI) to ensure that the cognate target sites are uniquely present in the mouse genome. Truncated (i.e., *mF9 Exon1 gRNA*[17] and *mF9 Exon6 gRNA*[17]) and full-length (i.e., *mF9 Exon1 gRNA*[20]) gRNAs were selected[34] based on these criteria that were designed to target either exon 1 or exon 6 of the mouse *F9* gene (Tables S1 and S2). All gRNAs were driven by a polymerase III (U6) promoter and cloned into an AAV vector. The corresponding AAV9-U6-mF9-Exon1-gRNA[20] (full-length gRNA), AAV9-U6-mF9-Exon1-gRNA[17] (truncated gRNA), and AAV9-U6-mF9-Exon6-gRNA[17] (truncated gRNA) vectors were produced and yielded normal vector titer (9×10^{12}–3×10^{13} vg/mL).

To selectively express Cas9 in the liver, we used a synthetic chimeric liver-specific promoter (designated as *HS-CRM8-TTRmin*) that was specifically designed to achieve high levels of hepatocyte-specific expression with no or only minimal ectopic expression in non-target tissues.[35,36] This robust liver-specific promoter was composed of a computationally designed hepatocyte-specific *cis*-regulatory module (*HS-CRM8*) coupled to a minimal transthyretin (*TTRmin*) promoter. One particularly attractive attribute of this *HS-CRM8* element is its small size (72 bp) and, in conjunction with the *TTRmin* (0.202 kb), allows for a 5- to 10-fold increase in gene expression. Consequently, this *HS-CRM8-TTRmin* promoter (0.27 kb) could be readily accommodated within a single-stranded (ss)AAV vector backbone to drive expression of a relatively large transgene like Cas9 (~4.2 kb). Typically, the titers of the corresponding AAV9-HS-CRM8-TTRmin-Cas9 vectors fell within the range of 3×10^{12} to 1×10^{13} vg/mL.

We performed various experiments to achieve somatic gene inactivation of the mouse *F9* gene. In the first experiment, we injected 6.25×10^{10} vg/mouse of the AAV9-HS-CRM8-TTRmin-Cas9 vector intravenously (i.v.) in neonatal C57BL/6 mice in combination with either the AAV9-U6-mF9-Exon1-gRNA[17] or AAV9-U6-mF9-Exon6-gRNA[17] vector (1.25×10^{11} vg/mouse i.v.). Neonatal C57BL/6 mice injected with AAV9-HS-CRM8-TTRmin-Cas9 and AAV9 encoding a scrambled gRNA (i.e., AAV9-U6-scrambled-gRNA) were used as controls. We next determined the biodistribution of the AAV9-HS-CRM8-TTRmin-Cas9 vector. qPCR analysis using primers specific for the synthetic *HS-CRM8-TTRmin* promoter revealed efficient transduction of the liver and, to a lesser extent, in other organs. In particular, vector copy number was 10-fold higher ($p < 0.05$) in the liver than in heart or brain. AAV copy numbers in skeletal muscle, spleen, lung, and kidney were typically less than 1% ($p < 0.001$) of what could be achieved in the liver (Figure 1). This biodistribution is consistent with the known transduction pattern of AAV9.[33,37]

CRISPR-Cas9-Mediated Somatic Inactivation of FIX Results in a Hemophilic Phenotype

In the first experiment, co-injection of the AAV9-HS-CRM8-TTRmin-Cas9 vector with either AAV9-U6-mF9-Exon1-gRNA[17] or AAV9-U6-mF9-Exon6-gRNA[17] resulted in a significant reduction of FIX activity levels (Figures 2A and 2B; $p < 0.01$) compared to controls injected with AAV9-HS-CRM8-TTRmin-Cas9 along with AAV9-U6-scrambled-gRNA. Two different doses of AAV9-HS-CRM8-TTRmin-Cas9 vector (i.e., 6.25×10^{10} vg/mouse or 1.25×10^{11} vg/mouse i.v.) and AAV9-U6-mF9-Exon1-gRNA[17], AAV9-U6-mF9-Exon6-gRNA[17] vector, or control AAV9-U6-scrambled-gRNA (i.e., 1.25×10^{11} vg/mouse or 2.5×10^{11} vg/mouse i.v.) were evaluated. Interestingly, the reduction of the FIX activity levels was

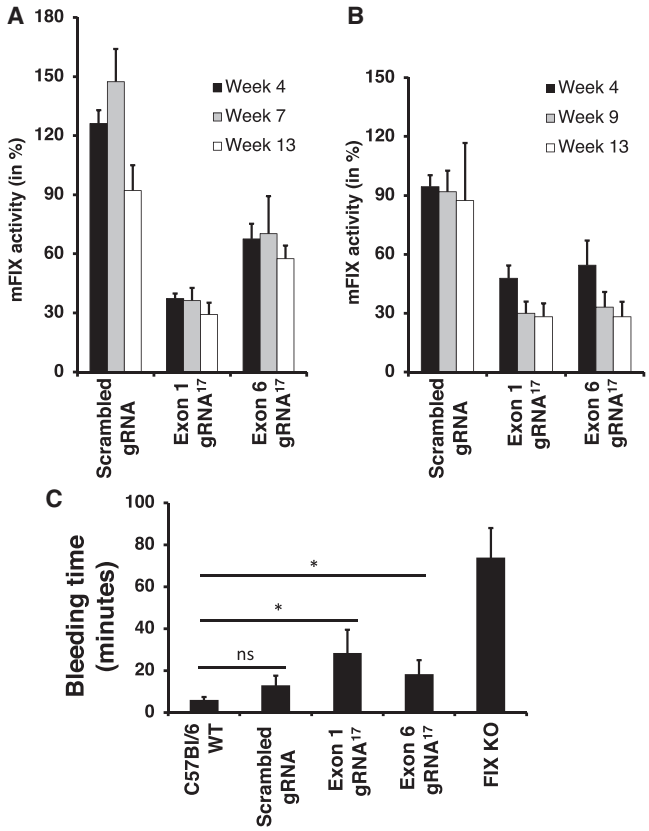

Figure 2. FIX Activity Levels and Bleeding Time after Gene Targeting with U6-mF9-Exon1-gRNA and U6-mF9-Exon6-gRNA

(A and B) For FIX activity levels (mean ± SD), two different doses of the AAV9-HS-CRM8-TTRmin-Cas9 vector (i.e., A, 6.25×10^{10} vg/mouse or B, 1.25×10^{11} vg/mouse i.v.) and AAV9-U6-mF9-Exon1- gRNA[17], AAV9-U6-mF9-Exon6-gRNA[17], or control AAV9-U6-scrambled-gRNA (i.e., A, 1.25×10^{11} vg/mouse or B, 2.5×10^{11} vg/mouse i.v.) were evaluated. FIX activity was determined using a functional FIX assay on mouse plasma obtained from the injected mice at distinct time points post-vector-injection. (C) Bleeding time (mean ± SD) after gene targeting with the AAV9-HS-CRM8-TTRmin-Cas9 vector (6.25×10^{10} vg/mouse i.v.) and AAV9-U6-mF9-Exon1- gRNA[17] or AAV9-U6-mF9-Exon6- gRNA[17] vector or control AAV9-U6-scrambled-gRNA (1.25×10^{11} vg/mouse i.v.) is shown. *$p < 0.05$ (Student's t-test); ns, not significant ($p > 0.1$).

more pronounced after gene targeting with U6-mF9-Exon1-gRNA[17] ($p < 0.01$) than with mF9-Exon6-gRNA[17] (Figures 2A and 2B) and could not be increased further by increasing the AAV9-HS-CRM8-TTRmin-Cas9 and AAV9-U6-mF9-Exon1-gRNA[17] vector doses. This suggests that saturation had been attained in the case of this mF9-Exon1-gRNA[17] targeting vector. However, increasing the AAV9-HS-CRM8-TTRmin-Cas9 and AAV9-U6-mF9-Exon6-gRNA[17] vector doses resulted in a further reduction in FIX activity levels until it was comparable to what could be attained with the AAV9-U6-mF9-Exon1-gRNA[17] vector. This suggests that the extent of the reduction in FIX activity—and hence the targeting efficiency—varies, depending on the intrinsic properties and/or target site of the gRNA. Most importantly, the loss of FIX activity after *in vivo* liver-directed editing with CRISPR/Cas9 was consistent with the emergence of a hemophilic phenotype (Figure 2C). In particular, co-injection of AAV9-HS-CRM8-TTRmin-Cas9 vector with either AAV9-U6-mF9-Exon1-gRNA[17] or AAV9-U6-mF9-Exon6-gRNA[17] in wild-type C57BL/6 mice resulted in a significant prolongation in bleeding time ($p < 0.05$). The effect on the bleeding diathesis was even more pronounced after gene targeting with U6-mF9-Exon1-gRNA[17] than with mF9-Exon6-gRNA[17] (Figure 2C), consistent with the observed differences in FIX activity levels at these vector doses (Figure 2A). Consequently, the FIX activity levels attained after CRISPR/Cas9-mediated *in vivo* targeting of the mouse *F9* gene correlated with the severity of the bleeding phenotype.

The use of truncated gRNAs was justified based on a previous report, demonstrating a decrease in off-target effects in transfected cell lines *in vitro* compared to when full-length gRNAs were employed.[34] Our initial experiments indicated that the gRNA targeting exon 1 of murine *F9* yielded the most robust decline in mFIX activity levels compared to the gRNA targeting exon 6. This was consistent with the highest frequency of insertions and deletions (indels) at this site. To compare the relative efficiency and specificity of truncated versus full-length gRNAs, we therefore designed AAV9 vectors expressing gRNAs that contain either 17 nt (truncated, designated as AAV9-U6-mF9-Exon1-gRNA[17]) or 20 nt (full-length, designated as AAV9-U6-mF9-Exon1-gRNA[20]) that are complementary to the same target sequence in exon 1 of the mouse *F9* gene (Figures 3A and 3B).

The AAV9-U6-mF9-Exon1-gRNAs encoding either the full-length 20 nt or truncated 17 nt gRNAs were co-injected with AAV9-HS-CRM8-TTRmin-Cas9 vector into either neonates (n = 6 per cohort; dose: 6.25×10^{10} vg/mouse of the AAV9-HS-CRM8-TTRmin-Cas9 and 1.25×10^{11} vg/mouse of AAV9-U6-mF9-Exon1-gRNA[17] or AAV9-U6-mF9-Exon1-gRNA[20] vector or AAV9-U6-scrambled-gRNA) or 4-week-old C57BL/6 mice (n = 3 per cohort; dose: 1.25×10^{11} vg/mouse of the AAV9-HS-CRM8-TTRmin-Cas9 and 2.50×10^{11} vg/mouse of AAV9-U6-mF9-Exon1-gRNA[17] or AAV9-U6-mF9-Exon1-gRNA[20] vector or AAV9-U6-scrambled-gRNA). Both full-length and truncated gRNAs reduced mFIX activity by approximately 50% (Figure 3C). The decline in FIX expression was sustained over 1 year after vector injection (data not shown). Similarly, the 4-week-old C57BL/6 mice with the CRISPR/Cas9 vectors, both the full-length and truncated gRNA, resulted in a significant reduction in FIX activity compared to PBS control or scrambled gRNA. There was no significant difference ($p = 0.11$) in targeting efficiency when comparing the 20 nt with the 17 nt gRNA (Figure 3D).

The reduction in FIX activity was relatively stable over time, indicating that long-term expression of Cas9 did not further enhance targeting efficiency (Figures 2A and 3C). We then tested the kinetics of Cas9 gene expression and gene copy number to assess whether Cas9 expression was sustained. This experiment was performed in C57BL/6 neonates where 6.25×10^{10} vg/mouse of the AAV9-HS-CRM8-TTRmin-Cas9 and 1.25×10^{11} vg/mouse of respective AAV9-U6-mF9-gRNA

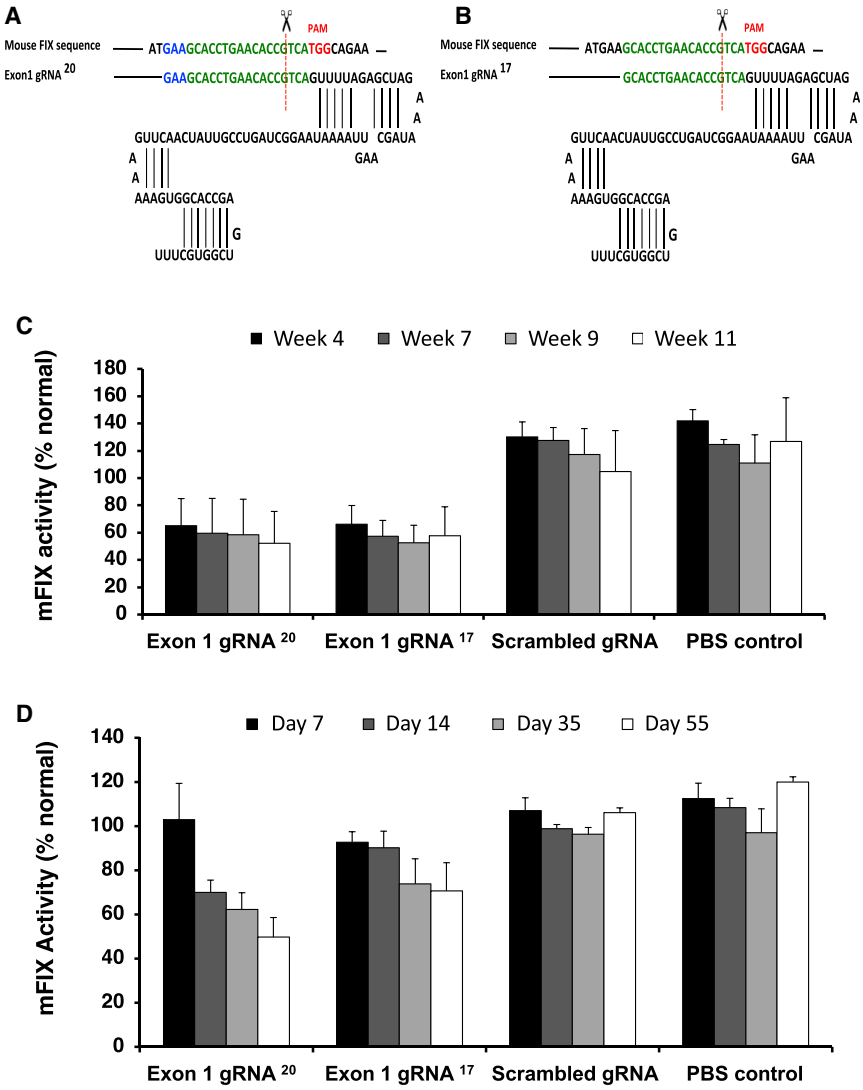

Figure 3. The gRNA Structures and FIX Activity Levels after Gene Targeting with U6-mF9-Exon1-gRNA^{17} and U6-mF9-Exon1-gRNA^{20} in Neonatal and 4-Week-Old Mice

(A and B) The detailed structure of the full-length 20-nt (exon1 gRNA^{20}) (A) and truncated 17-nt (exon1 gRNA^{17}) (B) gRNAs, respectively. (C) For FIX activity levels (mean ± SD) in neonates, the AAV9-HS-CRM8-TTRmin-Cas9 vector (6.25×10^{10} vg/mouse i.v.) and AAV9-U6-mF9-Exon1-gRNA^{17}, AAV9-U6-mF9-Exon1-gRNA^{20}, or control AAV9-U6-scrambled-gRNA (1.25×10^{11} vg/mouse i.v.) were evaluated. PBS-injected neonates were also used as control group. FIX activity was determined using a functional FIX assay on mouse plasma obtained from the injected mice at distinct time points post-vector-injection. (D) For FIX activity levels (mean ± SD) in 4-week-old mice, the AAV9-HS-CRM8-TTRmin-Cas9 vector (i.e.,1.25×10^{11} vg/mouse i.v.) and AAV9-U6-mF9-Exon1-gRNA^{17}, AAV9-U6-mF9-Exon1-gRNA^{20}, or control AAV9-U6-scrambled-gRNA (2.5×10^{11} vg/mouse i.v.) were evaluated. PBS-injected neonates were also used as control group. FIX activity was determined using a functional FIX assay on mouse plasma obtained from the injected mice at distinct time points post-vector-injection.

(exon 1 gRNA^{20}) was administered. The results showed that there is a significant reduction ($p < 0.05$) in the Cas9 copy number and mRNA expression over time (Figures 4A and 4B). This indicates that liver-specific expression of Cas9 is transient after AAV transduction in neonates. This represents an attractive "hit-and-go" scenario to maximize Cas9 expression and gene targeting during a critical window while preventing long-term expression of high levels of Cas9 protein. In addition, hepatic delivery and Cas9 expression, in either neonates or adults, may have contributed to immune tolerance to Cas9. This is consistent with previous reports demonstrating the potential of liver-directed gene therapy for immune tolerance induction, regardless of the vector used, in either neonates or adults.[38–40]

We conducted 3 independent experiments to determine both aspartate aminotransferase (AST) and alanine aminotransferase (ALT) levels in order to obtain comprehensive serum biochemistry. Two-day-old C57BL/6 neonates were injected with 6.25×10^{10} vg/mouse of the AAV9-HS-CRM8-TTRmin-Cas9 and 1.25×10^{11} vg/mouse of the respective AAV9-U6-mF9-gRNA vectors (Figures S1A and S1B), which was repeated with an independently produced vector batch (Figures S1C and S1D). Alternatively, 4-week-old C57BL/6 mice were injected with 1.25×10^{11} vg/mouse of the AAV9-HS-CRM8-TTRmin-Cas9 and 2.50×10^{11} vg/mouse of the respective AAV9-U6-mF9-gRNA vectors (Figures S1E and S1F). There was no significant elevation in AST and ALT levels, consistent with the lack of chronic liver inflammation or hepatotoxicity (Figure S1). In addition, we have tested for the presence anti-Cas9 antibodies in the plasma samples using a Cas9-specific ELISA at various time points. For all conditions, the levels of these antibodies were similar to the PBS-injected or scrambled-injected controls. This indicates there is no development of anti-Cas9 antibodies (Figure S2A). We have also conducted a comprehensive cytokine ELISA on plasma samples, testing for the presence of interleukin-1β (IL-1-β), IL-2, IL-6, IL-10, IL-12, interferon γ (IFN-γ), and tumor necrosis factor alpha (TNF-α). None of these cytokines were induced in the plasma of recipient mice 4 weeks after injection, consistent with the lack of any immune response against Cas9 (Figure S2B).

This further supports the notion that targeting the endogenous *F9* locus using either the AAV9-U6-mF9-Exon1-gRNA or AAV9-U6-mF9-Exon6-gRNA targeting constructs yielded no untoward hepatotoxicity or liver inflammation.

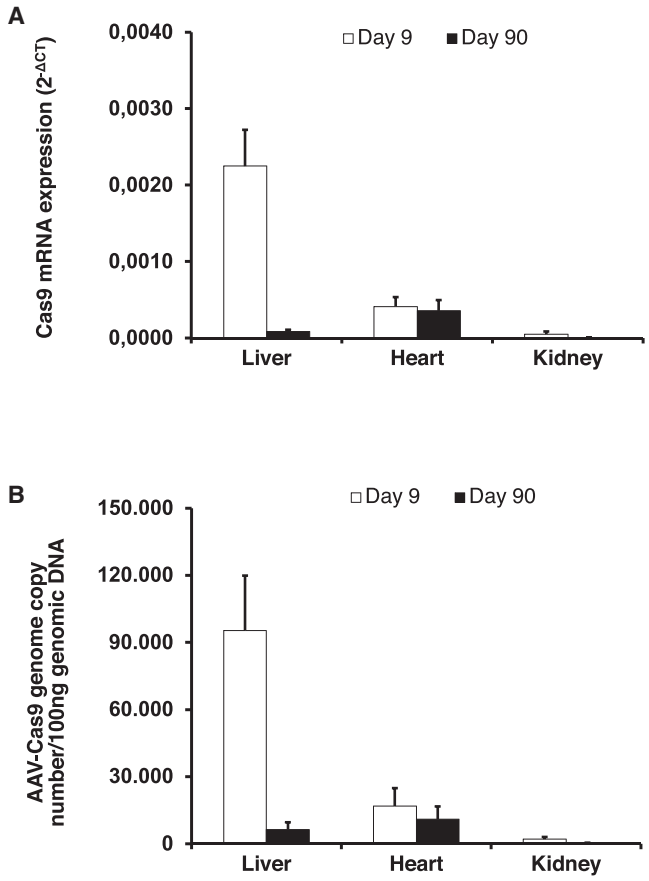

Figure 4. Cas9 Kinetic Analysis by Measuring mRNA Expression and Genomic DNA Copy Number in Liver, Heart, and Kidney

The AAV9-HS-CRM8-TTRmin-Cas9 vector (6.25×10^{10} vg/mouse i.v.) was co-injected with the AAV9-U6-mF9-Exon1-gRNA[20] (1.25×10^{11} vg/mouse i.v.), and the mRNA and genomic DNA expression was measured at day 9 and day 90 post-injection. (A) Cas9 mRNA expression (mean ± SD) was determined by qRT-PCR using primers specific for Cas9. Normalization was carried out using mouse GAPDH-specific primers. Cas9 expression was presented in terms of $2^{-\Delta CT}$ values. (B) Vector copy number (mean ± SD) was determined by qPCR using primers specific for the synthetic liver-specific *HS-CRM8-TTRmin* promoter driving Cas9 expression.

Analysis of Site-Specific *In Vivo* Editing Using the T7E1-Based Enzyme Mismatch Cleavage Method

To assess the targeting efficiency at the respective target sites in the mouse *F9* gene, we explored the use of an enzyme mismatch cleavage method based on the bacteriophage resolvase T7E1. The T7E1-based enzyme mismatch cleavage method assay takes advantage of the ability of T7E1 to cleave heteroduplex DNA at mismatches formed by single or multiple nucleotides. In contrast, cleavage activity of T7E1 is greater on mismatched than on Watson-Crick base pairs, though homoduplex DNA can be cleaved to a certain extent.[41,42] Hence, T7E1 is well suited to discriminate between homoduplex and heteroduplex double-stranded DNA (dsDNA). T7E1 analysis revealed that co-injection of the AAV9-HS-CRM8-TTRmin-Cas9 vector (6.25×10^{10} vg/mouse i.v.) with either AAV9-U6-mF9-Exon1-gRNA[17] or AAV9-U6-mF9-Exon6-gRNA[17] (1.25×10^{11} vg/mouse i.v.) resulted in a significant degree of heteroduplex dsDNA formation in the liver, consistent with the introduction of indels by NHEJ repair at the respective target loci in the mouse *F9* gene (designated as % indels in Figure 5 and Table 1). In particular, the extent of *F9* gene targeting in the liver was more pronounced after gene targeting with U6-mF9-Exon1-gRNA[17] (% indels: 42 ± 10) than with mF9-Exon6-gRNA[17] (% indels: 26 ± 21; Figure 5). This difference in targeting efficiency at the respective *F9* loci based on the two distinct gRNAs correlated with the differences in reduction of FIX activity (Figure 2A) and differences in prolongation of bleeding time (Figure 2C). In contrast, control mice injected with AAV9-HS-CRM8-TTRmin-Cas9 vector (6.25×10^{10} vg/mouse i.v.) with AAV9-U6-scrambled-gRNA (1.25×10^{11} vg/mouse i.v.) failed to yield any evidence of liver targeting in the *F9* gene based on the T7E1 assay, consistent with the lack of heteroduplex formation at the target locus (Figures 5A and 5C; lanes 9–11). Similarly, control mice not injected with any Cas9 or gRNA vectors did not exhibit any targeting based on the T7E1 assay (Figures 5A and 5C; lanes 1 and 2).

Indeed, there was no evidence of heteroduplex formation based on the T7E1 assay in heart or lungs of mice injected with AAV9-HS-CRM8-TTRmin-Cas9 and AAV9-U6-mF9-Exon1-gRNA[17] or AAV9-U6-mF9-Exon6-gRNA[17] (Table 1; Figures S5A–S5C).

Sequencing Analysis of On-Target and Off-Target Gene Editing

To independently confirm that the heteroduplexes detected using the T7E1-based enzyme mismatch cleavage method following *in vivo* CRIPSR/Cas9 gene delivery contained indels at the respective target sites in the *F9* locus, we performed sequencing analysis. Sanger sequencing of cloned PCR products derived from liver tissue revealed the presence of indels at the respective loci. In AAV9-HS-CRM8-TTRmin-Cas9 vector and AAV9-U6-mF9-Exon1-gRNA[17] co-injected mice, 4 out of 18 sequenced clones (22%) showed evidence of deletion and 3 out of 18 clones (17%) showed presence of insertions at the target site. In total, 7 out of 18 clones (39%) demonstrated the presence of indels (Figure S3). In AAV9-HS-CRM8-TTRmin-Cas9 vector and AAV9-U6-mF9-Exon6-gRNA[17] co-injected mice, 6 out of 19 sequenced samples showed evidence of deletion (5 small deletions and 1 large deletion; 32%) at the target site of mF9-Exon6 gRNA (Figure S3). These indels are consistent with the mechanism of action of CRISPR/Cas9-mediated gene editing, resulting in dsDNA breaks followed by NHEJ.[4,34] In contrast, PCR products obtained from control mice injected with AAV9-HS-CRM8-TTRmin-Cas9 vector (6.25×10^{10} vg/mouse i.v.) with AAV9-U6-scrambled-gRNA (1.25×10^{11} vg/mouse i.v.) did not show any evidence of indels.

Subsequently, a more comprehensive sequencing analysis was performed on the respective target loci in the *F9* gene. In particular, deep sequencing was first performed on the PCR products obtained from liver after *in vivo* CRISPR/Cas9 delivery. In mice co-injected with the AAV9-HS-CRM8-TTRmin-Cas9 (6.25×10^{10} vg/mouse

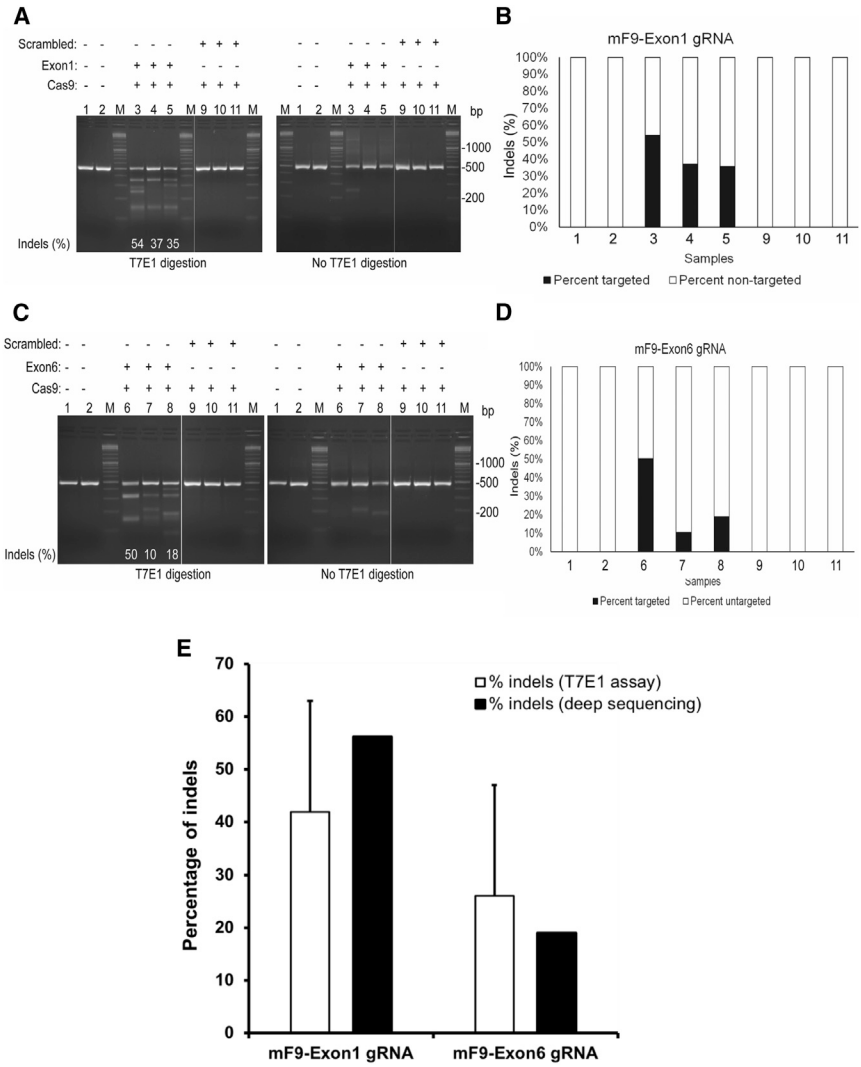

Figure 5. Assessment of AAV9-U6-mF9-Exon1-gRNA[17]- and AAV9-U6-mF9-Exon6-gRNA[17]-Induced Indels in Liver Genomic DNA Based on the T7E1-Based Enzyme Mismatch Cleavage Assay

(A) T7E1 digestion of PCR products at the mF9-Exon1-gRNA target site. Exon1 corresponds to mice injected with AAV9-U6-mF9-Exon1-gRNA[17] (1.25×10^{11} vg/mouse i.v.), scrambled corresponds to AAV9-U6-scrambled-gRNA-injected mice (1.25×10^{11} vg/mouse i.v.), and Cas9 corresponds to AAV9-HS-CRM8-TTRmin-Cas9-injected mice (6.25×10^{10} vg/mouse i.v.). (B) Densitometric quantification of bands in gel images of (A) to determine gene targeting efficiency is shown. Sample specifications: 1 and 2, wild-type C57BL/6 mice (no guide RNA or Cas9 vectors injected); 3, 4, and 5, mice co-injected with AAV9-HS-CRM8-TTRmin-Cas9 and AAV9-U6-mF9-Exon1-gRNA[17]; 9, 10, and 11, control mice co-injected with AAV9-HS-CRM8-TTRmin-Cas9 and AAV9-U6-scrambled-gRNA. M is the molecular weight ladder. (C) T7E1 digestion of PCR products at the mF9-Exon6-gRNA target site is shown. Exon6 corresponds to mice injected with AAV9-U6-mF9-Exon6-gRNA[17] (1.25×10^{11} vg/mouse i.v.), scrambled corresponds to AAV9-U6-scrambled-gRNA-injected mice (1.25×10^{11} vg/mouse i.v.), and Cas9 corresponds to AAV9-HS-CRM8-TTRmin-Cas9-injected mice (6.25×10^{10} vg/mouse i.v.). (D) Densitometric quantification of bands in gel images of (C) to determine gene targeting efficiency is shown. Sample specifications: 1 and 2, wild-type C57BL/6 mice (no guide RNA or Cas9 vectors injected); 6, 7, and 8, mice co-injected with AAV9-HS-CRM8-TTRmin-Cas9 and AAV9-U6-mF9-Exon6-gRNA[17] injected; 9, 10, and 11, control mice co-injected with AAV9-HS-CRM8-TTRmin-Cas9 and AAV9-U6-scrambled-gRNA. M is the molecular weight ladder. (E) Composite figure illustrating the percentage of indels (mean ± SD) assessed by T7E1-based enzyme mismatch cleavage assay and deep sequencing for both AAV9-U6-mF9-Exon1-gRNA[17] and AAV9-U6-mF9-Exon6-gRNA[17].

i.v.) and AAV9-U6-mF9-Exon1-gRNA[17] vectors (1.25×10^{11} vg/mouse i.v.), up to 56% sequence reads (based on a total of 655,818 reads) showed indels at the corresponding target site in exon 1 of the *F9* gene (Table 2; Figure S4A). Similarly, in mice co-injected with the AAV9-HS-CRM8-TTRmin-Cas9 vector (6.25×10^{10} vg/mouse i.v.) and AAV9-U6-mF9-Exon6-gRNA[17], up to 19% sequence reads (based on a total of 588,158 reads) showed indels at the corresponding target site in exon 6 of the *F9* gene. This suggests that targeting with the exon-1-specific gRNA was more efficient than with the exon-6-specific gRNA (Table 2; Figure S4B). This is consistent with the differences in heteroduplex formation based on the T7E1-based enzyme mismatch cleavage assay (Figure 5; Table 1), the differences in the extent of the reduction in FIX activity (Figures 2A and 2B), and the prolongation of bleeding time (Figure 2C). In contrast, control mice co-injected with AAV9-HS-CRM8-TTRmin-Cas9 (6.25×10^{10} vg/mouse i.v.) and AAV9-U6-scrambled-gRNA (1.25×10^{11} vg/mouse i.v.) failed to show any indels in these *F9* target loci. This is consistent with the T7E1 data (Figure 5) and reflects the hepatocyte specificity of the *HS-CRM8-TTRmin* promoter used to drive Cas9 expression (Table 1). Finally, on examining the deep sequencing data for putative top three off-target sites (Table S2) in liver genomic DNA of mice co-injected with AAV9-HS-CRM8-TTRmin-Cas9 vector (6.25×10^{10} vg/mouse i.v.) and either AAV9-U6-mF9-Exon1-gRNA[17] or AAV9-U6-mF9-Exon6-gRNA[17], no evidence for indels was visible (Table 2). This confirms the on-target specificity of the CRISPR/Cas9 system after *in vivo* gene delivery, which may be due to, at least in part, by the use of truncated gRNA.

In our next experiment comparing the full-length and truncated gRNA, the AAV9-U6-mF9-Exon1-gRNAs encoding either the full-length 20 nt or truncated 17 nt gRNAs were co-injected with AAV9-HS-CRM8-TTRmin-Cas9 vector into either neonates (n = 6 per cohort; dose: 6.25×10^{10} vg/mouse of the AAV9-HS-CRM8-TTRmin-Cas9 and 1.25×10^{11} vg/mouse of AAV9-U6-mF9-Exon1-gRNA[17] or AAV9-U6-mF9-Exon1-gRNA[20] vector or AAV9-U6-scrambled-gRNA). Both full-length and truncated gRNAs

Table 1. Frequencies of Guide RNAs Induced Indel Mutations at On-Target Sites in Mice Tissues as Determined by T7E1 Assay

gRNA ID Injected	Target ID	Gene	Genomic DNA	gRNA Target (17 nt) (5′–3′)	Mean % Indels ± SD[a]
Exon 1	*Exon1-gRNA*[17]	*F9*	liver	*GCACCTGAACACCGTCATGG*	42 ± 10
Exon 1	*Exon1-gRNA*[17]	*F9*	heart	*GCACCTGAACACCGTCATGG*	not detected
Exon 1	*Exon1-gRNA*[17]	*F9*	lung	*GCACCTGAACACCGTCATGG*	not detected
Exon 6	*Exon6-gRNA*[17]	*F9*	liver	*GACTTCACTCGAGTTGTTGG*	26 ± 21
Exon 6	*Exon6-gRNA*[17]	*F9*	heart	*GACTTCACTCGAGTTGTTGG*	not detected
Exon 6	*Exon6-gRNA*[17]	*F9*	lung	*GACTTCACTCGAGTTGTTGG*	not detected

[a]Mutation frequencies were assessed based on the T7E1 assay with means of triplicate measurements

reduced mFIX activity by approximately 50% (Figure 3C). This was independently confirmed by deep sequencing (Table 3). There was no significant difference in percentage indels obtained with the full-length or truncated gRNA at the target site in exon 1 of murine *F9*, consistent with the deep sequencing and mFIX expression data. The decline in FIX expression was sustained over 1 year after vector injection (data not shown).

DISCUSSION

In this study, we have validated and improved a CRISPR/Cas9-based AAV platform to achieve efficient and stable liver-specific gene targeting *in vivo* with a possible reduced risk of off-target effects in non-target genes and/or non-target tissues or organs. One of its key features is the incorporation of a computationally designed hepatocyte-specific synthetic promoter (designated as *HS-CRM8-TTRmin* promoter) to specifically direct high Cas9 expression levels in the liver. This promoter contains a 72-bp hepatocyte-specific *cis*-regulatory module (i.e., *HS-CRM8*) that is composed of a cluster of transcription factor binding site (TFBS) motifs characteristic of highly expressed liver-specific genes.[35,36] Most importantly, by virtue of its small size, this synthetic *de novo*-designed promoter allows for the incorporation of the *Streptococcus pyogenes* Cas9 (~4.2 kb) within an AAV backbone without compromising efficacy. The use of this small but potent synthetic promoter thereby overcomes some of the limitations that precluded the use of *S. pyogenes* Cas9 in AAV vectors, given its intrinsic packaging constraints. To assess the robustness of this approach, we estimated the efficacy of gene inactivation *in vivo* using coagulation *F9* as the target gene, and, as a proof of concept, we observed the bleeding phenotype consistent with hemophilia B. *In vivo* gene delivery of CRISPR/Cas9 using these hepatocyte-specific AAV did not provoke any hepatotoxicity, suggesting that it is a relatively safe approach for *in vivo* gene editing, supporting its use for potential clinical applications.

The targeting efficiency and specificity obtained with the current AAV-based approach compares favorably with that obtained using other strategies. In particular, *in vivo* delivery of CRISPR/Cas9 by hydrodynamic delivery resulted in relatively modest targeting efficiency,[27] necessitating *in vivo* selection of the gene-edited cells.[23] Our current approach is more efficient, obviating the need for such *in vivo* selection schemes to enrich for gene-editing cells. Although the use of hydrodynamic injection method can be beneficial for the generation of mouse models, this method is not well suited for human clinical applications, given the transient fluid overload and its impact on cardiac function.[43] Previous somatic *in vivo* gene delivery studies using AAV-based vectors expressing *S. pyogenes* Cas9 also resulted in relatively modest gene editing efficiencies, which were insufficient to yield a robust phenotype,[23] in contrast to our present study. This was likely due to, at least in part, the use of smaller promoters that were either relatively weak and/or not tissue specific.[23] The targeting efficiencies obtained with the current hepatocyte-specific AAV-based approach were comparable to the levels obtained with adenoviral vectors.[21] However, adenoviral vectors are known to provoke significant inflammatory responses following systemic administration[28,32] that can trigger liver toxicity, in contrast to when AAV vectors were employed.[35] This is compounded by the possible immune-adjuvant effect that may increase the risk of developing an immune response against the Cas9 protein and/or the Cas9-expressing cells.[20] Moreover, because most adenoviral vectors expressed Cas9 from a ubiquitously expressed *CMV* promoter, and because they exhibit a broad cellular tropism, this increases the risk of unwanted gene editing in non-target tissues.

Typically, therapeutic applications based on CRISPR/Cas9 rely on its ability to induce a dsDNA break in a DNA-sequence-specific manner, as determined by the gRNA sequence. In the absence of a homologous DNA donor template, this dsDNA break is repaired by NHEJ. This could result either in gene inactivation or gene repair, potentially restoring expression of a functional protein. If a homologous DNA donor template is provided, it can prompt homology-directed repair (HDR) at the dsDNA break, allowing replacement of the mutated with a corrected gene sequence. The ability to edit genes by either NHEJ or HDR critically depends on the efficiency of dsDNA cleavage at the desired locus. Our present study therefore focuses on this critical step in the gene editing process and shows that AAV-mediated delivery using *de novo*-designed liver-specific promoters allows for efficient liver-specific gene targeting, without any detectable off-target effects or adverse immune consequences, consistent with lack of anti-Cas9 antibodies or cytokine elevations. This paves the way toward future therapeutic liver-directed gene editing applications. Moreover, it also validates the current optimized system for animal modeling based on efficient and specific somatic liver-directed gene

Table 2. Frequencies of Guide RNAs Induced Indel Mutations at On- and Off-Target Sites in Mice Tissues as Determined by Deep Sequencing

gRNA ID Injected	Target ID	Gene	Genomic DNA	gRNA Target (17 nt) (5′–3′)	% of Reads Supporting an Indel
Exon 1	*Exon1-gRNA*[17]	*F9*	liver	*GCACCTGAACACCGTCATGG*	56
Exon 1	*Exon1-OT1*	–	liver	*GCACATGAACAGCGTCAGAG*	not detected
Exon 1	*Exon1-OT2*	–	liver	*GACCCTGAACACCCTCATGG*	not detected
Exon 1	*Exon1-OT3*	–	liver	*GTACCTGAACACCTTCTGAG*	not detected
Exon 6	*Exon6-gRNA*[17]	*F9*	liver	*GACTTCACTCGAGTTGTTGG*	19
Exon 6	*Exon6-OT1*	*Grin2b*	liver	*CACTTCACTCGAGTTGGGGG*	not detected
Exon 6	*Exon6-OT2*	–	liver	*CACTTCACTAGAGTTGTTAG*	not detected
Exon 6	*Exon6-OT3*	–	liver	*TACTACACTGGAGTTGTTGG*	not detected

inactivation. AAVs have recently been used for hepatic delivery of designer nucleases (i.e., zinc finger nucleases [ZFNs]) in patients suffering from a hereditary disease (i.e., Hunter syndrome).[44] Depending on the outcome of this trial, it is conceivable that the AAV platform may also be used in the future for hepatic delivery and expression of CRISPR/Cas9 components. Restricting expression of Cas9 in hepatocytes and obtaining sufficiently high levels to "maximize" gene targeting, as shown in the present study, is an important step toward achieving that goal.

AAVs offer many advantages over adenoviral vectors for clinical translation and animal modeling. Adenoviral delivery of CRISPR/Cas9 components resulted in inadvertent immune responses, such as Cas9-specific antibodies.[7] It is also known that adenoviral vectors, even helper-dependent vectors, can trigger T-cell-mediated clearance of gene-modified cells, including hepatocytes.[45] Consequently, these confounding immune variables may interfere with the interpretation of the consequences of CRISPR/Cas9 effects in mouse models. Moreover, it is well established that systemic administration of adenoviral vectors results in efficient transduction of innate immune effectors and consequently carries a substantial risk of liver inflammation, resulting in lethal consequences in trial subjects.[46] These disadvantages have severely hampered clinical applications based on adenoviral vectors. Furthermore, AAV-mediated CRISPR/Cas9-mediated targeting overcomes the intrinsic limitations of hydrodynamic delivery methods that were used to deliver the CRISPR/Cas9 components to the liver.[27]

Our current AAV-based study shows that the overall efficiency of CRISPR/Cas9-mediated gene targeting is far greater than what has been reported based on hydrodynamic CRISPR/Cas9 gene delivery that typically results in liver toxicity, excess fluid overload, and cardiac insufficiency. Consequently, relatively modest targeting efficiencies were obtained in the FIX gene by hydrodynamic gene delivery of the CRISPR/Cas components.[47–49]

In particular, recently, Guan and colleagues[47] showed that a *F9* mutation could be corrected *in vivo* by hydrodynamic tail vein injection of a plasmid encoding Cas9 and the single-guide RNA (sgRNA) along with either single-stranded oligodeoxynucleotide (ssODN; 120 nt) or long-donor DNA (with homology arms of 0.4 kb) containing the corrected sequence. A therapeutic effect could be obtained using both DNA donors, resulting in up to 0.56% and 1.5% of hepatocytes displaying a corrected genotype using ssODNs and the long DNA, respectively. A higher proportion of indels without correction was apparent, indicating DNA cleavage with NHEJ repair and without insertion of the donor DNA. Co-delivery of an adenoviral vector encoding Cas9 and a second one the sgRNA and the long DNA donor resulted in a high frequency of hepatocyte correction (5.5%), at least at early time points. However, no long-term correction of hemostasis was observed, which could mostly likely be due to the high inflammation in the liver and hepatocyte death provoked by the adenoviral vectors themselves.

The use of the hepatocyte-specific AAV-based CRISPR/Cas9 platform described in the present study therefore provides an attractive alternative that overcomes these limitations. Ultimately, the use of AAVs may also be preferred for ultimate clinical applications, given its attractive safety profile.[50] The current study provides a robust alternative to the use of smaller-sized Cas9 variants for AAV delivery.[22] However, these Cas9 variants were not yet tested *in vivo* in combination with the truncated gRNAs with higher specificity.

Some studies suggest that SaCas9 seems to work with similar efficiency to SpCas9, at least *in vitro*, and that the extent of off-target effects is comparable (*ibid.*),[51] though this may vary depending on the gRNA,[52] requiring comprehensive head-to-head comparative studies. However, one of the advantages of SaCas9 is its smaller size of 3.3 kb. This enables the incorporation of both the Cas9 and gRNA expression cassettes in a single AAV vector. It is encouraging that SaCas9 has been used to achieve relatively efficient gene targeting in the *F9* gene, resulting in a therapeutic effect in hemophilic mice.[53]

However, there are also a number of limitations associated with the use of SaCas9, which justifies the exploration of SpCas9-based applications in parallel, for *in vivo* somatic gene inactivation. First, second-generation, high-fidelity SpCas9 derivatives (designated as SpCas9-HF1) have been developed that harbor alterations designed to reduce non-specific DNA contacts.[54] SpCas9-HF1 retains on-target activities comparable to wild-type SpCas9 but rendered all or nearly all

Table 3. Frequencies of Guide RNAs Induced Indel Mutations at On- and Off-Target Sites in Mice Tissues as Determined by Deep Sequencing Comparing Truncated (17 nt) and Full-Length (20 nt) gRNAs

gRNA ID Injected	Target ID	Gene	Genomic DNA	gRNA Target (17 nt and 20 nt) (5′–3′)	% of Reads Supporting an Indel[a]
Exon 1	*Exon1 gRNA*[17]	*F9*	liver	*GCACCTGAACACCGTCATGG*	34.98
Exon 1	*Exon1-OT1*	–	liver	*GCACATGAACAGCGTCAGAG*	0.01–0.1
Exon 1	*Exon1-OT2*	–	liver	*GACCCTGAACACCCTCATGG*	0.01–0.1
Exon 1	*Exon1-OT3*	–	liver	*GTACCTGAACACCTTCTGAG*	0.01–0.1
Exon 1	*Exon1 gRNA*[20]	*F9*	liver	*GAAGCACCTGAACACCGTCATGG*	40.10
Exon 1	*Exon1-OT1*	–	liver	*GCACATGAACAGCGTCAGAG*	0.01–0.1
Exon 1	*Exon1-OT2*	–	liver	*GACCCTGAACACCCTCATGG*	0.01–0.1
Exon 1	*Exon1-OT3*	–	liver	*GTACCTGAACACCTTCTGAG*	0.01–0.1

[a]The control liver samples obtained by injecting scrambled gRNA were also sequenced for the OT1/OT2/OT3 and resulted in no significant indel reads (0.01%−0.1%).

off-target events undetectable by genome-wide break capture and targeted sequencing methods. Hence, this SpCas9 derivative is considered one of the most precise Cas9 versions available to date and can readily be accommodated in our liver-specific AAV vector containing the computationally designed hepatocyte-specific promoter. Second, the available SpCas9 sites (i.e., *NGG*) are more frequent in the genome than for SaCas9 (i.e., *NNGRRT*), providing more opportunities to identify specific Cas9 cleavage sites for gene inactivation or to facilitate HDR. Moreover, the commonly used SpCas9 can be modified to recognize alternative PAM sequences beyond the prototypical *NGG* consensus.[55] In particular, other SpCas9 variants were generated that exhibit improved specificity in human cells, possessing better discrimination against off-target sites with non-canonical *NAG* and *NGA* PAMs and/or mismatched spacers (*ibid.*). Third, the aforementioned Ran et al.[22] study did not include a head-to-head comparative analysis of SaCas9 versus SpCas9 targeting efficiency and specificity *in vivo*. Moreover, in some cases, only 5% indels could be detected following *in vivo* liver-directed targeting with the all-in-one SaCas9 vector.[22] This justifies the need for further comprehensive comparative *in vivo* analyses of hepatic targeting with SaCas9 versus SpCas9 and its derivatives.

Consequently, somatic gene inactivation with SpCas9 and its derivatives has its merits and can be considered a valuable alternative to SaCa9-based applications. In our current study, the novelty is based primarily on the use of a small yet robust computationally designed hepatocyte-specific synthetic promoter to drive Cas9 in an AAV vector. Moreover, to our knowledge, this is the first *in vivo* study comparing the efficiency and specificity of truncated gRNA for *in vivo* SpCas9-mediated targeting. This allowed us to achieve relatively efficient somatic *in vivo* hepatic targeting, resulting in a distinctive hemophilic phenotype with no detectable off-target effects and with specific targeting effects in the liver only. The current platform is therefore well suited to express SpCas9 and its next-generation variants with higher fidelity and/or altered PAM specificities. In search of smaller Cas9 enzymes for efficient *in vivo* delivery by AAVs, short Cas9s were also identified from the *CRISPR1* locus of *Streptococcus thermophilus* LMD-9 (St1Cas9; ~3.3 kb)[1] as well as a rationally designed truncated form of SpCas9.[56] However, both systems have important practical drawbacks: the former requires a complex *PAM* sequence (*NNAGAAW*),[57] which restricts the range of accessible targets, whereas the latter exhibits significantly reduced activity. Hence, the performance of smaller Cas9 variants is not necessarily better compared to the original SpCas9 or its next-generation derivatives.

All of the previously published *in vivo* somatic CRISPR/Cas9 editing studies relied on the use of non-truncated gRNAs, which are known to yield a higher frequency of non-specific off-target editing *in vitro* and *in vivo*.[29,31,34] In contrast, our current strategy relies on the use of truncated gRNAs, which were previously shown to improve the specificity of Cas9 targeting to the desired genomic locus and reduce off-target editing, though based largely on *in vitro* studies in cell lines.[34]

The present study now extends the use of these truncated gRNAs with increased targeting specificity for *in vivo* applications. We have conducted an *in vivo* comparison of the full-length (20 nt) and truncated (17 nt) gRNAs targeting Exon1 of murine *F9* in both neonates and 4-week-old mice, which had not been done previously. This comprehensive *in vivo* analysis revealed that both the full-length and truncated gRNAs significantly reduced mFIX activity compared to the control groups. This indicates that, for this locus, the full-length and truncated gRNAs yielded comparable gene targeting efficiencies as confirmed by FIX levels and percentage of sequence reads supporting indels. Hence, it is encouraging that truncated gRNAs are at least as efficient as full-length gRNAs.

Using a previously developed computational algorithm, we identified several putative off-target sites.[30] We then assessed the frequency of reads supporting indels at the top 3 ranked putative off-target sites by deep sequencing. In contrast to the gRNA target sites in exon 1 and exon 6 of the *F9* gene (Table 2), we found no evidence of genome editing in these putative off-target sites (detection limit of Illumina deep sequencing—0.095%)[58] when the truncated gRNAs are employed, as in the case of full-length gRNAs. This further supports the specificity of the truncated gRNAs. Fu et al.[34] have also shown that not all truncated gRNAs have improved specificity compared

to full-length gRNAs. Additionally, they showed that some of the tested gRNAs have no detectable off-target effects for both full-length and truncated gRNAs, consistent with our results. Hence, the impact of truncated gRNAs on targeting efficiency and specificity cannot be generalized and would need to be tested on a case-by-case basis. Nevertheless, there is still a need to further refine the computational algorithms for prediction of off-target sites. Alternatively, a comprehensive assessment of off-target sites based on sensitive *in vivo* detection assays would need to be developed. This is challenging and is beyond the scope of the current study. This could potentially be accomplished using an adaptation of the GUIDE-seq approach,[59] which relies on the capture of double-stranded oligonucleotides into dsDNA breaks. Alternatively, integration-defective lentiviral vectors could be employed.[38,60]

The current CRISPR/Cas9-based approach offers new opportunities to achieve rapid, efficient, and specific genome targeting in liver and may facilitate functional genomics studies without necessarily having to rely on transgenic mouse models. The generation of transgenic mice is time consuming and costly, especially if it requires complex breeding schemes to combine mutations in different genes. The current validation of an efficient and specific CRISPR/Cas9-mediated *in vivo* targeting strategy in hepatocytes may facilitate and expedite the creation of complex disease models by inactivating multiple genes based on gRNA multiplexing.[1,61,62] Ultimately, this versatile and improved CRISPR/Cas9-based system has potentially broad implications for the field and may pave the way toward the treatment of genetic, acquired, or infectious liver diseases by either NHEJ or HDR.[2,6,21,23,24,27,63,64]

MATERIALS AND METHODS

Construction of CRISPR/Cas9 AAV Vectors

The *Streptococcus pyogenes* Cas9 (no. 41815; Addgene)[4] was cloned in single-stranded AAV vector AAVss-HS-CRM8-TTRmin-MCS-SV40polyA[35] at *XbaI/AgeI* restriction sites, which was subsequently confirmed by Sanger sequencing. The DNAs corresponding to the selected truncated gRNAs that target exon 1 and exon 6 of the mouse *F9* gene (i.e., *mF9 Exon 1*: *GCACCTGAACACCGTCA*; *mF9 Exon 6*: *GACTTCACTCGAGTTGT*) and the scrambled control (*GGGTCTTCGAGAAGACCT*) were cloned into a gRNA cloning vector (no. 41824; Addgene).[4] The scrambled gRNA is identical, as previously described by Anderson and colleagues[27] and was used as a negative control gRNA. Briefly, the gRNA cloning vector was linearized using *AflII* restriction enzyme. The oligos were designed, annealed, and extended using Phusion Hot Start II high-fidelity DNA polymerase (F549S; Life Technologies), according to the supplier's instructions. These 100-bp oligos were subsequently cloned into the *AflII*-linearized gRNA cloning vector. The resulting vector was then digested by XhoI/NotI, and the fragment was then cloned into the corresponding site of the AAV vector designated as AAVss-HS-CRM8-TTRmin-MCS-SV40polyA,[35] which was sequence verified.

The oligos used for cloning of the mF9 targeting gRNAs were as follows: U6-mF9-Exon1-gRNA (targets exon 1 of the mouse *F9* gene): 5′-TTTCTTGGCTTTATATATCTTGTGGAAAGGACGAAACACCGCACCTGAACACCGTCA-3′, 5′-GACTAGCCTTATTTTAACTTGCATTTCTAGCTCTAAAACTGACGGTGTTCAGGTGC-3′; U6-mF9-Exon6-gRNA (targets exon 6 of mouse *F9* gene): 5′-TTTCTTGGCTTTATATATCTTGTGGAAAGGACGAAACACCGACTTCACTCGAGTTGT-3′, 5′-GACTAGCCTTATTTTAACTTGCTATTTCTAGCTCTAAAACACAACTCGAGTGAAGTC-3′; and U6-scrambled-gRNA (negative control gRNA): 5′-TTTCTTGGCTTTATATATCTTGTGGAAAGGACGAAACACCGGGTCTTCGAGAAGACCT-3′, 5′-GACTAGCCTTATTTTAACTTGCTATTTCTAGCTCTAAAACAGGTCTTCTCGAAGACCC-3′.

The final scrambled control plasmid obtained from above steps was then used as the vector backbone to generate the full-length gRNAs that target exon 1 (i.e., *mF9 Exon 1*: *GAAGCACCTGAACACCGTCA*). A fragment flanked with NdeI/XbaI containing this 20-nt gRNA sequence was generated (Geneart; Life Technologies, Europe) and cloned using the same restriction sites in the scrambled gRNA control plasmid.

Vector Production and Purification

To produce the AAV serotype 9 vectors, AAV-293 cells were cotransfected using calcium phosphate (Invitrogen, Carlsbad, CA, USA) with the AAV plasmid of interest, a chimeric packaging construct, and an adenoviral helper plasmid, as described previously.[33] Cells were harvested two days post-transfection and lysed by successive freeze/thaw cycles and sonication, followed by Benzonase (Novagen, Madison, WI, USA) and deoxycholic acid (Sigma Aldrich, St. Louis, MO, USA) treatments and 3 consecutive rounds of cesium chloride (Invitrogen, Carlsbad, CA, USA) density gradient ultracentrifugation. Fractions containing the AAV vector particles were collected and dialyzed in Dulbecco's PBS (GIBCO, BRL) containing 1 mM $MgCl_2$. Quantitative real-time PCR with SYBR Green and primers for the HS-CRM8-TTRmin (Cas9 vector) or U6 promoter (gRNAs) were used to determine vector titers. The HS-CRM8-TTRmin forward primer sequence was *5′-GGAGGCTGCTGGTGAATATT-3′* and the reverse primer sequence was *5′- TCCAAACCTGCTGATTCTG-3′*. The U6 forward primer sequence was *5′-GCAGGCTTTAAAGGAACCAA-3′* and the reverse primer sequence was *5′- ACTGCAAACTACCCAAGAAAT-3′*. To generate the standard curves, known copy numbers of the corresponding vector plasmids were used.

Animals

The animal experiments were approved by the University's Animal Ethics Committee. C57BL/6 mice (Taconic, Denmark; Janvier Labs, France) were used in this study. One- to 2-day-old neonatal mice were injected into the facial vein with two different doses of the AAV9-HS-CRM8-TTRmin-Cas9 vector (i.e., 6.25×10^{10} vg/mouse or 1.25×10^{11} vg/mouse i.v.) and AAV9-U6-mF9-Exon1-gRNA[20], AAV9-U6-mF9-Exon1-gRNA[17], AAV9-U6-mF9-Exon6-gRNA[17], or control AAV9-U6-scrambled-gRNA (i.e., 1.25×10^{11} vg/mouse or 2.5×10^{11} vg/mouse i.v.). The ratio of Cas9 to gRNA vectors was kept constant (i.e., 1:2) at both vector doses.[65]

Also, 4-week-old mice were injected into tail vein with AAV9-HS-CRM8-TTRmin-Cas9 vector (1.25×10^{11} vg/mouse i.v.) and AAV9-U6-mF9-Exon1-gRNA[20], AAV9-U6-mF9-Exon1-gRNA[17], or control AAV9-U6-scrambled-gRNA (2.5×10^{11} vg/mouse i.v.). The ratio of Cas9 to gRNA vectors was kept constant (i.e., 1:2).

To obtain plasma samples, whole blood was collected at regular intervals into buffered citrate, followed by centrifugation at 4°C, 13,000 rpm for 4 min. To obtain serum samples, blood was collected by phlebotomy of the retro-orbital plexus using non-heparinized capillaries and allowed to clot for 1 or 2 hr, followed by centrifugation. FIX activity was determined in plasma using a Factor IX chromogenic assay (BIOPHEN, Hyphen BioMed, France), according to the manufacturer's protocol. For the standard curve, plasma from age-matched non-injected C57BL/6 mice was used. AST and ALT activity was determined in serum using AST (MAK055-1KT, Sigma-Aldrich, MO, USA) and ALT activity assay kits (MAK052-1KT, Sigma-Aldrich, MO, USA), according to the manufacturer's protocol. The cytokine levels were measured using the Mouse Inflammatory Cytokines Multi-Analyte ELISA Array (MEM-004A, QIAGEN Benelux B.V, Belgium), according to manufacturer's protocol. The anti-Cas9 antibody levels were analyzed using a modified ELISA protocol.[25,66] Briefly, ninety-six-well Nunc flat-bottom plates (Thermo Scientific) were coated with the SpCas9 protein (0.5 μg/well; PNA Bio; cat no. CP01) in 1× coating buffer (Coating Solution Concentrate Kit; KPL) overnight at 4°C. The plates were then washed with 1× wash buffer diluted from 20× Wash Solution (KPL) and blocked with 1% BSA Blocking Solution (KPL) for 1 hr at room temperature. Mouse plasma was diluted 40-fold with 1% BSA Diluent Solution (KPL), added to the wells, and incubated for 1 hr at room temperature with shaking (200 rpm). The mouse monoclonal antibody against SpCas9 (Epigentek; clone 7A9; cat no. A-9000-100) was serially diluted and used as a standard to quantify immunoglobulin G1 (IgG1). After washing, each well was incubated with 100 μL of horseradish peroxidase (HRP)-labeled goat anti-mouse IgG1 (Santa Cruz Biotechnology; diluted 1:4,000) for 1 hr at room temperature. The wells were washed four times and incubated with 100 μL of ABTS ELISA HRP Substrate (KPL). Optical density at 410 nm was measured using a microplate reader. The IgG1 standard curve was generated using the four-parameter logistic regression equation (4PL). Bleeding time was assessed using a tail-clip assay. Briefly, mice were anesthetized and the tail was placed in pre-warmed 37°C normal saline solution for 2 min and subsequently cut at 2 or 3 mm diameter. The tail was then immediately placed in 37°C saline solution, and mice were monitored to assess the bleeding time.

Biodistribution and Copy Number Analysis

Genomic DNA was extracted from different tissues using the DNeasy Blood and Tissue Kit (QIAGEN, Chatsworth, CA, USA). 100 ng DNA was analyzed using qPCR ABI Prism 7900HT (Applied Biosystems, Foster City, CA, USA) with *HS-CRM8-TTR*-specific primers *5′-GGAGGCTGCTGGTGAATATT-3′* (forward) and *5′-TCCAAACCTGCTGATTCTG-3′* (reverse). To generate standard curves, known copy numbers of the corresponding vector plasmid was used. The mRNA was isolated from different organs using a NucleoSpin RNA extraction kit (Machery-Nagel, Germany). Using a *cDNA* synthesis kit (Invitrogen, Carlsbad, CA, USA), 250 ng of RNA from each organ was reverse transcribed to *cDNA*. *cDNA* was then analyzed by qPCR ABI Prism 7900HT (Applied Biosystems, Foster City, CA, USA) using Cas9-specific primers *5′-GTGCCCCAGTCTTTTCTCA-3′* (forward) and *5′-CAACTCAGACAGGCCACCT-3′* (reverse). The expression levels were normalized to murine glyceraldehyde-3-phosphate dehydrogenase (*GAPDH*) *mRNA* expression, obtained by using the forward primer *5′-TGTGTCCGTCGTGGATCTGA-3′* and reverse primer *5′-GCCTGCTTCACCACCTTCTTGA-3′*. Cas9 expression levels based on the $2^{-\Delta CT}$ method were determined in the organs of mice injected with AAV9-HS-CRM8-TTRmin-Cas9 vector (6.25×10^{10} vg/mouse i.v.) and AAV9-U6-mF9-Exon1[20] gRNA (i.e., 1.25×10^{11} vg/mouse i.v.).

T7E1-Based Enzyme Mismatch Cleavage Assay

PCR reactions were performed using Phusion Hot Start II high-fidelity DNA polymerase (F549S; Life Technologies), using the respective PCR primers and conditions (see below and Table S3). For the T7E1 assay on the target site of *mF9-Exon1-gRNA*, primers *T7E1-mF9-Exon1-F/R* and *Nested2-T7E1-Exon1-F/R* were used, and for the T7E1 assay on the target site of *mF9-Exon6-gRNA*, primers *T7E1-Ex6-Pair2-mF9-F/R* and *Nested6Ex6Pair2F/R* were used. All tested loci amplified successfully using nested PCR. PCR products were analyzed on a 3% agarose gel to verify both size and purity and were run with a DNA marker (SM0331; Fermentas) for size reference. The PCR products were subjected to denaturation and reannealing using a S1000 thermocycler (Bio-Rad). The cycle conditions used for denaturation and reannealing were 95°C for 2 min, ramp at 2°C per second until 85°C was reached followed by 85°C for 2 min, ramp at 0.1°C per second until 25°C (Table S3), 25°C for 2 min, and then kept at 16°C until used for T7E1 digestion. T7E1 digestion was done at 37°C for 20 min, along with undigested controls. The resulting products were run on 3% agarose gel to observe evidence for indels. Genome editing efficiencies were determined by densitometric quantification of the gel bands using NIH ImageJ 1.49.

DNA Sequencing of CRISPR/Cas9-Induced Indel Mutations

The nested PCR products obtained by the T7E1 assay were first subjected to Sanger sequencing. PCR products were purified using ExoSAP-IT (78250; Affymatrix) and were cloned into Zero Blunt TOPO vector (K2875-J10; Life Technologies). The plasmid DNAs were isolated using pureyield plasmid miniprep system (A1222; Promega). Plasmids were sequenced using an M13 forward primer (5′-GTAAAACGACGGCCAG-3′) by the Sanger sequencing method (GATC, Germany). Subsequently, the gRNA target sites in the *F9* gene and their respective predicted top three off-target sites (Tables S1 and S2), as predicted by the algorithm from the Zhang lab (http://crispr.mit.edu/) were subjected to deep sequencing. Briefly, the PCRs were done at the *mF9-Exon1-gRNA* and *mF9-Exon6-gRNA* target sites and the predicted top three off-target sites, using the respective primers (Table S4). PCR reactions were done using

Phusion Hot Start II high-fidelity DNA polymerase (F549S; Life Technologies) to generate PCR products of size 200–230 bp. The PCR products were purified by QIAquick PCR Purification Kit (catalog no. 28104; QIAGEN). The resulting PCR products were sequenced and analyzed using the MiSeq PE150 platform (BGI, Europe). Raw image files were processed by Illumina pipeline for base calling with default parameters, and the sequences of each individual were generated as 150-bp paired-end reads. The 150-bp paired-end reads were subjected to bioinformatics analysis.

Bioinformatics Analysis of Deep Sequencing Data

The bioinformatics analysis began from the sequencing data (raw data), which were generated from the Illumina pipeline. First, the adaptor sequence in the raw data was removed, and low quality reads that have too many undefined nucleotides or low base quality were discarded. This step produced the "clean data". Second, Burrows-Wheeler Aligner (BWA) was used to do the alignment. BWA gave the result in BAM format files. The BAM format files were further processed, such as fixing mate information of the alignment, adding read group information and removing duplicate reads caused by PCR. For qualitative analysis, we used IGV 2.3.59 for viewing BAM files aligned at on-target and off-target sites with mouse reference genome (mm10). The indels were considered to be caused due to the gRNA, if they were localized within 10 bp of its expected cut site. This cut site was assumed to be around 3 bp upstream of the CRISPR/Cas9 PAM sequence. For quantitative analysis of BAM files, we used the web-interface-based cloud computing platform Biostar Galaxy (https://usegalaxy.org).[50] The web interface of galaxy could be used to run command-line-driven tools, such as samtools. The individual target sequences were made as BED files, which contained the chromosomal positions of targeted sites. The BED files were used for alignment with BAM files to recognize presence of indels. The BED files and BAM files were uploaded to the server of https://usegalaxy.org to perform the analysis. Then, "mpileup" under NGS:samtools was run on each BAM file to calculate the percentage of indels, with mouse (*Mus musculus*): mm10 assembly as reference genome. Genotype likelihood computation was performed with v*cf.* as output format. The v*cf.* filter was applied to the v*cf.* dataset generated using mpileup to create the dataset containing indels. The parameters used for analysis of indels can be found at https://usegalaxy.org/u/ksingh/w/copy-of-indel-analysis-workflow-constructed-from-history-mf9-analysis. These v*cf.* datasets provided indels, if any, at the targeted site along with the maximum fraction of reads supporting an indel (IMF; i.e., maximum fraction of reads supporting an indel). The IMF values were multiplied by 100 to get the maximum percentage of reads supporting an indel.

Statistics

To analyze data, Microsoft Excel Statistics package was used. Values shown in the figures are mean ± SD. Statistical significance was determined using Student's t test. For kinetic studies, statistics were performed using a repeated-measure two-way ANOVA.

SUPPLEMENTAL INFORMATION

Supplemental Information includes five figures and six tables and can be found with this article online at https://doi.org/10.1016/j.ymthe.2018.02.023.

AUTHOR CONTRIBUTIONS

K.S. designed the gRNAs and cloning, performed the T7E1 assays, and conducted the bio-informatics analysis. H.E., M.Y.R., E.S.-K., S.S., and N.N. produced and characterized the vector. H.E., N.N., and E.S.-K. performed the animal experiments. M.Y.R. and N.N. performed the biodistribution and expression analyses. K.S., N.N., H.E., and M.Y.R. contributed to the writing of the manuscript. M.K.C. and T.V. designed and managed the experiments, coordinated the work, and wrote the manuscript. T.V. and M.K.C. are joint senior corresponding authors. K.S., H.E., and N.N. are joint first authors.

CONFLICTS OF INTEREST

T.V. and M.K.C. have filed and granted patent applications on the use of liver-specific cis-regulatory modules.

ACKNOWLEDGMENTS

This study was supported by grants from the Fonds voor Wetenschappelijke Onderzoek (FWO), Stichting tegen Kanker (STK), the VUB Strategic Research Program "Groeier," the VUB Industrieel Onderzoeksfonds (Groups of Expertise in Applied Research [GEAR]), and the VUB Proof of Concept Grant (Industrieel Onderzoeksfonds) to M.K.C. and T.V. M.Y.R. is a recipient of a Fundación Cardiovascular de Colombia/Colciencias Fellowship and an AFM PhD Fellowship. N.N. is an FWO postdoctoral fellow.

REFERENCES

1. Cong, L., Ran, F.A., Cox, D., Lin, S., Barretto, R., Habib, N., Hsu, P.D., Wu, X., Jiang, W., Marraffini, L.A., and Zhang, F. (2013). Multiplex genome engineering using CRISPR/Cas systems. Science *339*, 819–823.
2. Ding, Q., Strong, A., Patel, K.M., Ng, S.L., Gosis, B.S., Regan, S.N., Cowan, C.A., Rader, D.J., and Musunuru, K. (2014). Permanent alteration of PCSK9 with in vivo CRISPR-Cas9 genome editing. Circ. Res. *115*, 488–492.
3. Jinek, M., Chylinski, K., Fonfara, I., Hauer, M., Doudna, J.A., and Charpentier, E. (2012). A programmable dual-RNA-guided DNA endonuclease in adaptive bacterial immunity. Science *337*, 816–821.
4. Mali, P., Yang, L., Esvelt, K.M., Aach, J., Guell, M., DiCarlo, J.E., Norville, J.E., and Church, G.M. (2013). RNA-guided human genome engineering via Cas9. Science *339*, 823–826.
5. Platt, R.J., Chen, S., Zhou, Y., Yim, M.J., Swiech, L., Kempton, H.R., Dahlman, J.E., Parnas, O., Eisenhaure, T.M., Jovanovic, M., et al. (2014). CRISPR-Cas9 knockin mice for genome editing and cancer modeling. Cell *159*, 440–455.
6. Anguela, X.M., Sharma, R., Doyon, Y., Miller, J.C., Li, H., Haurigot, V., Rohde, M.E., Wong, S.Y., Davidson, R.J., Zhou, S., et al. (2013). Robust ZFN-mediated genome editing in adult hemophilic mice. Blood *122*, 3283–3287.
7. Wang, H., Yang, H., Shivalila, C.S., Dawlaty, M.M., Cheng, A.W., Zhang, F., and Jaenisch, R. (2013). One-step generation of mice carrying mutations in multiple genes by CRISPR/Cas-mediated genome engineering. Cell *153*, 910–918.
8. Zhu, Z., Verma, N., González, F., Shi, Z.-D., and Huangfu, D. (2015). A CRISPR/Cas-mediated selection-free knockin strategy in human embryonic stem cells. Stem Cell Reports *4*, 1103–1111.
9. Hai, T., Teng, F., Guo, R., Li, W., and Zhou, Q. (2014). One-step generation of knockout pigs by zygote injection of CRISPR/Cas system. Cell Res. *24*, 372–375.

10. Li, D., Qiu, Z., Shao, Y., Chen, Y., Guan, Y., Liu, M., Li, Y., Gao, N., Wang, L., Lu, X., et al. (2013). Heritable gene targeting in the mouse and rat using a CRISPR-Cas system. Nat. Biotechnol. *31*, 681–683.

11. Liang, P., Xu, Y., Zhang, X., Ding, C., Huang, R., Zhang, Z., Lv, J., Xie, X., Chen, Y., Li, Y., et al. (2015). CRISPR/Cas9-mediated gene editing in human tripronuclear zygotes. Protein Cell *6*, 363–372.

12. Qin, W., Dion, S.L., Kutny, P.M., Zhang, Y., Cheng, A.W., Jillette, N.L., Malhotra, A., Geurts, A.M., Chen, Y.G., and Wang, H. (2015). Efficient CRISPR/Cas9-mediated genome editing in mice by zygote electroporation of nuclease. Genetics *200*, 423–430.

13. Hendel, A., Bak, R.O., Clark, J.T., Kennedy, A.B., Ryan, D.E., Roy, S., Steinfeld, I., Lunstad, B.D., Kaiser, R.J., Wilkens, A.B., et al. (2015). Chemically modified guide RNAs enhance CRISPR-Cas genome editing in human primary cells. Nat. Biotechnol. *33*, 985–989.

14. Mandal, P.K., Ferreira, L.M., Collins, R., Meissner, T.B., Boutwell, C.L., Friesen, M., Vrbanac, V., Garrison, B.S., Stortchevoi, A., Bryder, D., et al. (2014). Efficient ablation of genes in human hematopoietic stem and effector cells using CRISPR/Cas9. Cell Stem Cell *15*, 643–652.

15. Hou, Z., Zhang, Y., Propson, N.E., Howden, S.E., Chu, L.F., Sontheimer, E.J., and Thomson, J.A. (2013). Efficient genome engineering in human pluripotent stem cells using Cas9 from Neisseria meningitidis. Proc. Natl. Acad. Sci. USA *110*, 15644–15649.

16. Xue, H., Wu, J., Li, S., Rao, M.S., and Liu, Y. (2016). Genetic modification in human pluripotent stem cells by homologous recombination and CRISPR/Cas9 system. Methods Mol. Biol. *1307*, 173–190.

17. Wu, Y., Zhou, H., Fan, X., Zhang, Y., Zhang, M., Wang, Y., Xie, Z., Bai, M., Yin, Q., Liang, D., et al. (2015). Correction of a genetic disease by CRISPR-Cas9-mediated gene editing in mouse spermatogonial stem cells. Cell Res. *25*, 67–79.

18. Nakamura, K., Fujii, W., Tsuboi, M., Tanihata, J., Teramoto, N., Takeuchi, S., Naito, K., Yamanouchi, K., and Nishihara, M. (2014). Generation of muscular dystrophy model rats with a CRISPR/Cas system. Sci. Rep. *4*, 5635.

19. Tu, Z., Yang, W., Yan, S., Guo, X., and Li, X.-J. (2015). CRISPR/Cas9: a powerful genetic engineering tool for establishing large animal models of neurodegenerative diseases. Mol. Neurodegener. *10*, 35.

20. Tucker, B.A., Mullins, R.F., and Stone, E.M. (2014). Stem cells for investigation and treatment of inherited retinal disease. Hum. Mol. Genet. *23* (R1), R9–R16.

21. Cheng, R., Peng, J., Yan, Y., Cao, P., Wang, J., Qiu, C., Tang, L., Liu, D., Tang, L., Jin, J., et al. (2014). Efficient gene editing in adult mouse livers via adenoviral delivery of CRISPR/Cas9. FEBS Lett. *588*, 3954–3958.

22. Ran, F.A., Cong, L., Yan, W.X., Scott, D.A., Gootenberg, J.S., Kriz, A.J., Zetsche, B., Shalem, O., Wu, X., Makarova, K.S., et al. (2015). In vivo genome editing using Staphylococcus aureus Cas9. Nature *520*, 186–191.

23. Senís, E., Fatouros, C., Große, S., Wiedtke, E., Niopek, D., Mueller, A.-K., Börner, K., and Grimm, D. (2014). CRISPR/Cas9-mediated genome engineering: an adeno-associated viral (AAV) vector toolbox. Biotechnol. J. *9*, 1402–1412.

24. Swiech, L., Heidenreich, M., Banerjee, A., Habib, N., Li, Y., Trombetta, J., Sur, M., and Zhang, F. (2015). In vivo interrogation of gene function in the mammalian brain using CRISPR-Cas9. Nat. Biotechnol. *33*, 102–106.

25. Wang, D., Mou, H., Li, S., Li, Y., Hough, S., Tran, K., Li, J., Yin, H., Anderson, D.G., Sontheimer, E.J., et al. (2015). Adenovirus-mediated somatic genome editing of Pten by CRISPR/Cas9 in mouse liver in spite of Cas9-specific immune responses. Hum. Gene Ther. *26*, 432–442.

26. Zuckermann, M., Hovestadt, V., Knobbe-Thomsen, C.B., Zapatka, M., Northcott, P.A., Schramm, K., Belic, J., Jones, D.T., Tschida, B., Moriarity, B., et al. (2015). Somatic CRISPR/Cas9-mediated tumour suppressor disruption enables versatile brain tumour modelling. Nat. Commun. *6*, 7391.

27. Yin, H., Xue, W., Chen, S., Bogorad, R.L., Benedetti, E., Grompe, M., Koteliansky, V., Sharp, P.A., Jacks, T., and Anderson, D.G. (2014). Genome editing with Cas9 in adult mice corrects a disease mutation and phenotype. Nat. Biotechnol. *32*, 551–553.

28. Jooss, K., and Chirmule, N. (2003). Immunity to adenovirus and adeno-associated viral vectors: implications for gene therapy. Gene Ther. *10*, 955–963.

29. Fu, Y., Foden, J.A., Khayter, C., Maeder, M.L., Reyon, D., Joung, J.K., and Sander, J.D. (2013). High-frequency off-target mutagenesis induced by CRISPR-Cas nucleases in human cells. Nat. Biotechnol. *31*, 822–826.

30. Hsu, P.D., Scott, D.A., Weinstein, J.A., Ran, F.A., Konermann, S., Agarwala, V., Li, Y., Fine, E.J., Wu, X., Shalem, O., et al. (2013). DNA targeting specificity of RNA-guided Cas9 nucleases. Nat. Biotechnol. *31*, 827–832.

31. Cho, S.W., Kim, S., Kim, Y., Kweon, J., Kim, H.S., Bae, S., and Kim, J.S. (2014). Analysis of off-target effects of CRISPR/Cas-derived RNA-guided endonucleases and nickases. Genome Res. *24*, 132–141.

32. DiMattia, M.A., Nam, H.J., Van Vliet, K., Mitchell, M., Bennett, A., Gurda, B.L., McKenna, R., Olson, N.H., Sinkovits, R.S., Potter, M., et al. (2012). Structural insight into the unique properties of adeno-associated virus serotype 9. J. Virol. *86*, 6947–6958.

33. Vandendriessche, T., Thorrez, L., Acosta-Sanchez, A., Petrus, I., Wang, L., Ma, L., DE Waele, L., Iwasaki, Y., Gillijns, V., Wilson, J.M., et al. (2007). Efficacy and safety of adeno-associated viral vectors based on serotype 8 and 9 vs. lentiviral vectors for hemophilia B gene therapy. J. Thromb. Haemost. *5*, 16–24.

34. Fu, Y., Sander, J.D., Reyon, D., Cascio, V.M., and Joung, J.K. (2014). Improving CRISPR-Cas nuclease specificity using truncated guide RNAs. Nat. Biotechnol. *32*, 279–284.

35. Chuah, M.K., Petrus, I., De Bleser, P., Le Guiner, C., Gernoux, G., Adjali, O., Nair, N., Willems, J., Evens, H., Rincon, M.Y., et al. (2014). Liver-specific transcriptional modules identified by genome-wide in silico analysis enable efficient gene therapy in mice and non-human primates. Mol. Ther. *22*, 1605–1613.

36. Nair, N., Rincon, M.Y., Evens, H., Sarcar, S., Dastidar, S., Samara-Kuko, E., Ghandeharian, O., Man Viecelli, H., Thöny, B., De Bleser, P., et al. (2014). Computationally designed liver-specific transcriptional modules and hyperactive factor IX improve hepatic gene therapy. Blood *123*, 3195–3199.

37. Zincarelli, C., Soltys, S., Rengo, G., and Rabinowitz, J.E. (2008). Analysis of AAV serotypes 1-9 mediated gene expression and tropism in mice after systemic injection. Mol. Ther. *16*, 1073–1080.

38. Mátrai, J., Cantore, A., Bartholomae, C.C., Annoni, A., Wang, W., Acosta-Sanchez, A., Samara-Kuko, E., De Waele, L., Ma, L., Genovese, P., et al. (2011). Hepatocyte-targeted expression by integrase-defective lentiviral vectors induces antigen-specific tolerance in mice with low genotoxic risk. Hepatology *53*, 1696–1707.

39. Matsui, H., Shibata, M., Brown, B., Labelle, A., Hegadorn, C., Andrews, C., Chuah, M., VandenDriessche, T., Miao, C.H., Hough, C., and Lillicrap, D. (2009). A murine model for induction of long-term immunologic tolerance to factor VIII does not require persistent detectable levels of plasma factor VIII and involves contributions from Foxp3+ T regulatory cells. Blood *114*, 677–685.

40. Mingozzi, F., Liu, Y.L., Dobrzynski, E., Kaufhold, A., Liu, J.H., Wang, Y., Arruda, V.R., High, K.A., and Herzog, R.W. (2003). Induction of immune tolerance to coagulation factor IX antigen by in vivo hepatic gene transfer. J. Clin. Invest. *111*, 1347–1356.

41. Babon, J.J., Youil, R., and Cotton, R.G. (1995). Improved strategy for mutation detection–a modification to the enzyme mismatch cleavage method. Nucleic Acids Res. *23*, 5082–5084.

42. Youil, R., Kemper, B.W., and Cotton, R.G. (1995). Screening for mutations by enzyme mismatch cleavage with T4 endonuclease VII. Proc. Natl. Acad. Sci. USA *92*, 87–91.

43. Suda, T., and Liu, D. (2007). Hydrodynamic gene delivery: its principles and applications. Mol. Ther. *15*, 2063–2069.

44. Kaiser, J (2017). A human has been injected with gene-editing tools to cure his disabling disease. Here's what you need to know. http://www.sciencemag.org/news/2017/11/human-has-been-injected-gene-editing-tools-cure-his-disabling-disease-here-s-what-you.

45. Chuah, M.K., Schiedner, G., Thorrez, L., Brown, B., Johnston, M., Gillijns, V., Hertel, S., Van Rooijen, N., Lillicrap, D., Collen, D., et al. (2003). Therapeutic factor VIII levels and negligible toxicity in mouse and dog models of hemophilia A following gene therapy with high-capacity adenoviral vectors. Blood *101*, 1734–1743.

46. Raper, S.E., Chirmule, N., Lee, F.S., Wivel, N.A., Bagg, A., Gao, G.P., Wilson, J.M., and Batshaw, M.L. (2003). Fatal systemic inflammatory response syndrome in a ornithine transcarbamylase deficient patient following adenoviral gene transfer. Mol. Genet. Metab. *80*, 148–158.

47. Guan, Y., Ma, Y., Li, Q., Sun, Z., Ma, L., Wu, L., Wang, L., Zeng, L., Shao, Y., Chen, Y., et al. (2016). CRISPR/Cas9-mediated somatic correction of a novel coagulator factor IX gene mutation ameliorates hemophilia in mouse. EMBO Mol. Med. *8*, 477–488.

48. Huai, C., Jia, C., Sun, R., Xu, P., Min, T., Wang, Q., Zheng, C., Chen, H., and Lu, D. (2017). CRISPR/Cas9-mediated somatic and germline gene correction to restore hemostasis in hemophilia B mice. Hum. Genet. *136*, 875–883.

49. Nguyen, T.H., and Anegon, I. (2016). Successful correction of hemophilia by CRISPR/Cas9 genome editing in vivo: delivery vector and immune responses are the key to success. EMBO Mol. Med. *8*, 439–441.

50. Nathwani, A.C., Reiss, U.M., Tuddenham, E.G., Rosales, C., Chowdary, P., McIntosh, J., Della Peruta, M., Lheriteau, E., Patel, N., Raj, D., et al. (2014). Long-term safety and efficacy of factor IX gene therapy in hemophilia B. N. Engl. J. Med. *371*, 1994–2004.

51. Zhang, X., Liang, P., Ding, C., Zhang, Z., Zhou, J., Xie, X., Huang, R., Sun, Y., Sun, H., Zhang, J., et al. (2016). Efficient production of gene-modified mice using Staphylococcus aureus Cas9. Sci. Rep. *6*, 32565.

52. Friedland, A.E., Baral, R., Singhal, P., Loveluck, K., Shen, S., Sanchez, M., Marco, E., Gotta, G.M., Maeder, M.L., Kennedy, E.M., et al. (2015). Characterization of Staphylococcus aureus Cas9: a smaller Cas9 for all-in-one adeno-associated virus delivery and paired nickase applications. Genome Biol. *16*, 257.

53. Ohmori, T., Nagao, Y., Mizukami, H., Sakata, A., Muramatsu, S.I., Ozawa, K., Tominaga, S.I., Hanazono, Y., Nishimura, S., Nureki, O., and Sakata, Y. (2017). CRISPR/Cas9-mediated genome editing via postnatal administration of AAV vector cures haemophilia B mice. Sci. Rep. *7*, 4159.

54. Kleinstiver, B.P., Pattanayak, V., Prew, M.S., Tsai, S.Q., Nguyen, N.T., Zheng, Z., and Joung, J.K. (2016). High-fidelity CRISPR-Cas9 nucleases with no detectable genome-wide off-target effects. Nature *529*, 490–495.

55. Kleinstiver, B.P., Prew, M.S., Tsai, S.Q., Topkar, V.V., Nguyen, N.T., Zheng, Z., Gonzales, A.P., Li, Z., Peterson, R.T., Yeh, J.R., et al. (2015). Engineered CRISPR-Cas9 nucleases with altered PAM specificities. Nature *523*, 481–485.

56. Nishimasu, H., Ran, F.A., Hsu, P.D., Konermann, S., Shehata, S.I., Dohmae, N., Ishitani, R., Zhang, F., and Nureki, O. (2014). Crystal structure of Cas9 in complex with guide RNA and target DNA. Cell *156*, 935–949.

57. Garneau, J.E., Dupuis, M.E., Villion, M., Romero, D.A., Barrangou, R., Boyaval, P., Fremaux, C., Horvath, P., Magadán, A.H., and Moineau, S. (2010). The CRISPR/Cas bacterial immune system cleaves bacteriophage and plasmid DNA. Nature *468*, 67–71.

58. Li, J.Z., Chapman, B., Charlebois, P., Hofmann, O., Weiner, B., Porter, A.J., Samuel, R., Vardhanabhuti, S., Zheng, L., Eron, J., et al.; ACTG A5262 Study Team (2014). Comparison of illumina and 454 deep sequencing in participants failing raltegravir-based antiretroviral therapy. PLoS ONE *9*, e90485.

59. Tsai, S.Q., Zheng, Z., Nguyen, N.T., Liebers, M., Topkar, V.V., Thapar, V., Wyvekens, N., Khayter, C., Iafrate, A.J., Le, L.P., et al. (2015). GUIDE-seq enables genome-wide profiling of off-target cleavage by CRISPR-Cas nucleases. Nat. Biotechnol. *33*, 187–197.

60. Gabriel, R., Lombardo, A., Arens, A., Miller, J.C., Genovese, P., Kaeppel, C., Nowrouzi, A., Bartholomae, C.C., Wang, J., Friedman, G., et al. (2011). An unbiased genome-wide analysis of zinc-finger nuclease specificity. Nat. Biotechnol. *29*, 816–823.

61. Kabadi, A.M., Ousterout, D.G., Hilton, I.B., and Gersbach, C.A. (2014). Multiplex CRISPR/Cas9-based genome engineering from a single lentiviral vector. Nucleic Acids Res. *42*, e147.

62. Sakuma, T., Nishikawa, A., Kume, S., Chayama, K., and Yamamoto, T. (2014). Multiplex genome engineering in human cells using all-in-one CRISPR/Cas9 vector system. Sci. Rep. *4*, 5400.

63. Li, H., Haurigot, V., Doyon, Y., Li, T., Wong, S.Y., Bhagwat, A.S., Malani, N., Anguela, X.M., Sharma, R., Ivanciu, L., et al. (2011). In vivo genome editing restores haemostasis in a mouse model of haemophilia. Nature *475*, 217–221.

64. Park, C.Y., Kim, D.H., Son, J.S., Sung, J.J., Lee, J., Bae, S., Kim, J.H., Kim, D.W., and Kim, J.S. (2015). Functional correction of large factor VIII gene chromosomal inversions in hemophilia A patient-derived iPSCs using CRISPR-Cas9. Cell Stem Cell *17*, 213–220.

65. Yang, Y., Wang, L., Bell, P., McMenamin, D., He, Z., White, J., Yu, H., Xu, C., Morizono, H., Musunuru, K., et al. (2016). A dual AAV system enables the Cas9-mediated correction of a metabolic liver disease in newborn mice. Nat. Biotechnol. *34*, 334–338.

66. Chew, W.L., Tabebordbar, M., Cheng, J.K., Mali, P., Wu, E.Y., Ng, A.H., Zhu, K., Wagers, A.J., and Church, G.M. (2016). A multifunctional AAV-CRISPR-Cas9 and its host response. Nat. Methods *13*, 868–874.